detritus | Multidisciplinary Journal for Circular Economy and Sustainable Management of Residues

CISA

A PRELIMINARY STUDY ON REAL-TIME ASBESTOS RECOGNITION IN TUNNEL SPOIL OF GREEN STONES

Sergio Malinconico [1], Federica Paglietti [1,*], Sergio Bellagamba [1], Silvia Serranti [2], Giuseppe Bonifazi [2], Davide Gattabria [2], Ivano Lonigro [3] and Riccardo Gasbarrone [3]

[1] *Department of new technologies for occupational safety of industrial plants, products and human settlements, Italian Workers' Compensation Authority (INAIL-DIT), via R. Ferruzzi 38/40, Rome, Italy*
[2] *Department of Chemical Engineering, Materials and Environment, Sapienza - University of Rome, via Eudossiana 18, 00184 Rome, Italy*
[3] *Research and Service Center for Sustainable Technological Innovation (Ce.R.S.I.Te.S.), Sapienza - University of Rome, Viale XXIV Maggio 7, 04100 Latina, Italy*

Article Info:
Received:
27 May 2024
Revised:
4 September 2024
Accepted:
4 October 2024
Available online:
19 November 2024

Keywords:
Mineral fibers
Environmental monitoring
Reflectance spectroscopy
Microscopy
Waste valorization

ABSTRACT

This study focuses on the analysis of serpentinite rocks to detect asbestos minerals, with a particular emphasis at discriminating chrysotile from other minerals and matrices (antigorite, lizardite) in serpentinites. The primary objective of this exploratory study is to lay the groundwork for the development of an innovative system for real-time identification of asbestos on the surface of materials and rocks. In more detail, the study emphasizes the advantages of utilization of rapid and reliable portable instrumentation, aided by machine learning (ML) techniques. Serpentinite rock debris from tunnel excavation activities (i.e. tunnel spoil) were collected at the Cravasco railway tunnelling site (Genoa - Italy) of the TEN-T Rhine-Alps Core Corridor. On-site analysis was conducted using the ASD FieldSpec 4 Standard-Res spectrophotoradiometer (350-2500 nm). A two-class classifier was developed based on acquired reflectance spectra, to discriminate between the "Presence of asbestiform fibers" and the "Absence of asbestiform fibers". The classification model was calibrated through stereomicroscopic inspection and electron microscopy carried on selected sample fractions.

1. INTRODUCTION

The economic grow is leading to an increasingly interconnected world, with the development of new infrastructures. However, the alteration of natural ecosystems may cause significant environmental and health risks, that must be carefully assessed and monitored. In the context of the circular economy paradigm, a sustainable management is needed, aimed at preventing the production of waste and the misusage of resources. To this end, during earth/rocks excavation (e.g., tunneling works) it could be very useful to carry out a fast characterization of spoils, that could allow the real-time sorting of materials. This can be a complex task, considering the high heterogeneity of natural matrices.

In the case of Green Stones (GS), the presence of Naturally Occurring Asbestos (NOA) minerals constitutes a serious health risk. Therefore, to ascertain the presence of asbestos fibers is crucial to distinguish between by-product (i.e., inert) and hazardous waste; the latter requiring specific and expensive environmental and safety measures (Voit et al., 2020). In European Countries, if the excavated material contains more than 0.1% of asbestos fibers, it is compulsory classified as hazardous waste and landfilled (Paglietti et al., 2016).

The GS are a group of mafic and ultramafic metamorphic rocks of magmatic origin made up of different lithotypes, including serpentinites, mainly used as inert materials or ornamental stones (Carmignano et al., 2019). Asbestos is a common constituent, but the mineralogic composition depends on regional-local geological conditions. In Italy, chrysotile and tremolite asbestos occur often within serpentinites, the former being the most common one (Bloise et al., 2014). Since it has the same chemical composition as antigorite and lizardite (i.e., not-fibrous serpentines), the analysis is complex and is usually carried out in laboratories with expensive instruments (mainly electron microscopes) and procedures that require many hours for sample preparation and analysis to get reliable results (Lee et al., 2008). During spectroscopic analysis, many minerals such as talc, chlorite, balangeroite and carlosturanite can interfere and bias the results (Olori et al., 2017). In this context, new tools and instruments can be tested, which are more and more available for material

* Corresponding author:
Federica Paglietti
email: f.paglietti@inail.it

https://doi.org/10.31025/2611-4135/2024.19441

analyses, including Machine Learning (ML) techniques applied on sensor-generated data (Bonifazi et al., 2019a; Neo et al., 2022).

We describe a preliminary study carried on with a promising real-time technique based on reflectance spectroscopy, calibrated through standard analytical methodologies, that has previously showed to allow an affordable automatic recognition of asbestos inside anthropic materials (Bonifazi et al., 2019b). The study focuses on serpentinite-based debris coming from tunneling excavations in Cravasco, near Genoa (Liguria Region-Italy), where two sections of the Genoa - Milan high-speed railway line are under construction. The section is called "Unico Terzo Valico di Giovi - Nodo di Genova" and is a portion of the Rhine-Alps Core Corridor (one of the main European railway lines). The tunneling activities began in 2014 and should be completed by 2035 (Webuild-RFI, 2021). As chrysotile was found, the executive projects were specifically adapted, including strict safety procedures (IMT, 2024). At first, the excavated material is placed inside a three-stage confinement (internal storage), then it is moved to a further static confinement with greater capacity (external storage), from which the waste is progressively sent to landfills, while the uncontaminated sub-products are deposited in an adjacent disused quarry.

2. MATERIALS AND METHODS

2.1 Sampling

In September 2023, twenty-four samples were taken from the Cravasco tunneling site, specifically from the following areas/lots: 1) quarry front, 2) internal contaminated debris deposit, 3) internal uncontaminated debris deposit, 4) external contaminated storage. The sample's number and location were chosen to obtain composed samples that are representative of the four investigated areas. Two different approaches were followed for sampling from the piles:

- at the internal storages and the excavation front, due to complex operating conditions (static and dynamically confined environment, instability of the front, difficulty in transporting large quantities of sample) an incremental approach was used, taking at least 5 aliquots in different points for each sample;
- at the external storage, considering the larger volume stored, the lower safety risks and the proximity to site facilities, a greater number of samples was preferred, each consisting of a single increment, taken in different points of the storage, both on the horizontal and vertical plane.

The materials present different grain sizes (from decimetric blocks to silt) and are mainly composed by serpentinites. Within individual lithoid blocks, a compact matrix is recognizable, made by either dark-grained or bright green, or bluish minerals, interconnected with friable veins and aggregates with light shade-whitish colors (Figure 1a). The humidity is extremely variable, and few samples are composed mainly by mud. Sometimes, anthropic materials used in the work were present, such as cement and artificial vitreous fibers, especially in the quarry front. In detail, the 24 samples are reported in Table 1.

2.2 On-site reflectance spectra acquisition

On-site, 50 to 100 reflectance spectra were acquired for each sample using the ASD FieldSpec 4 Standard-Res portable spectrophotoradiometer, that operates in the Vis–SWIR regions (350-2500 nm) with a spectral resolution of 3 nm at 700 nm and 10 nm at 1400/2100 nm. The spectra were acquired in different positions on the sample's surface, to collect most of the radiometric (i.e., compositional) variations. To avoid cross and hazardous contamination, a borate glass was placed between the sample and the probe. Data acquisition and calibration procedure were performed using RS3 software (Ver. 6.2).

2.3 Stereomicroscopy

In laboratory, representative fractions (sub-samples) were manually taken from each sample, via homogenization and coning – quartering procedures. To carry out a fast qualitative analysis by stereomicroscopy, a sub-sample set were inserted inside borosilicate glass Petri dishes (Figure 1b). The capsules were sealed with plasticine, parafilm and/or adhesive tape, for safety reasons. The instrument used was a Leica M205C equipped with an Axiocam208 digital camera, that allows to determine the main morphological parameters of the elongated particles, such as aspect ratio, color and presence of fibrils diverging from a bundle, thus resulting in a screening for asbestos fibers.

2.4 Analysis of the fine fraction

Another sub-sample set was separated by considering the sampling area (e.g., the quarry front) to get fast qualitative results via state-of-art Scanning Electron Microscopy with Energy-Dispersion Spectroscopy (SEM-EDS). The unified sub-samples were dried at 110°C, then sieved with a sieve shaker (Retsch GmbH AS200) to separate the < 106 µm size particles - that was assumed to contain most of the eventual asbestos. SEM-EDS was performed with a Carl Zeiss GmbH Evo MA15 operating at 20 kV in high vacuum and mounting a X-Max model X-ray detector (Oxford Instruments) with a resolution of 127 eV at 5.9 KeV. To separate and analyze the particles, dispersions at 1% concentration were prepared with distilled water, then aliquots containing 0.1 mg for each sample were filtered onto 0.2 µm pore-size polycarbonate membranes (IMH, 1994). After drying at room temperature in a bell jar glass desiccator, filter portions were finally attached to aluminum stubs and sputtered with gold.

2.5 Analysis of reflectance spectra

Data files acquired on-site with the portable spectrophotoradiometer were converted into ASCII text files using ViewSpec Pro, then imported and analyzed in MATLAB (Ver. 9.12; The Mathworks, Inc., Natick, Massachusetts, United States) environment with PLS_toolbox (Ver. 8.2; Eigenvector Research, Inc Manson, Washington, United States). At first, a 2nd Derivative algorithm (Savitzky–Golay (S-G) filter) and a Mean Center algorithm were applied on

TABLE 1: Samples list and information.

Sample ID	Sampling area	Info
CRA01	External deposit	Block with ~20 cm size and smaller fragments
CRA02	External deposit	Fragment with ~10 cm size and smaller fragments
CRA03	External deposit	Mud, fragment with ~5 cm size and smaller fragments
CRA04	External deposit	Block with ~25 cm size and smaller fragments
CRA05	External deposit	Fragments with ~5 cm size and smaller fragments
CRA06	External deposit	Fragment with ~8 cm size and smaller fragments
CRA07	External deposit	Fragment with ~10 cm size
CRA08	External deposit	Fragment with ~3 cm size
CRA09	External deposit	Fragment with ~3 cm size
CRA10	External deposit	Fragment with ~10 cm size and smaller fragments
CRA11	External deposit	Fragment with ~5 cm size and smaller fragments
CRA12	External deposit	Fragment with < 3 cm size
CRA13	External deposit	Mud, fragment with ~5 cm size and smaller fragments
CRA14	External deposit	Mud, fragment with ~5 cm size and smaller fragments
CRA15	Quarry front	Concrete with wire and fragments < 5 cm
CRA16	Quarry front	Mud with wire and fragments < 5 cm
CRA17	Quarry front	Fragment with ~15 cm size and smaller fragments
CRA18	Quarry front	Fragment with ~8 cm size and smaller fragments
CRA19	Quarry front	Fragment with ~10 cm size and smaller fragments
CRA20	Quarry front	Fragments with < 3 cm size, cement and reinforcing glass fibers
CRA21	Internal deposit with asbestos	Mud with fragments with < 3 cm size
CRA22	Internal deposit without asbestos	Fragments with < 5 cm size and cement
CRA23	Internal deposit with asbestos	Fragments with < 7 cm size
CRA24	Quarry front	Reinforcing glass fibers bar

the averaged sample spectra. After pre-processing, a Principal Component Analysis (PCA) was carried out to relate the variance between reflectance spectra to qualitative data acquired with microscopy (Wold et al., 1987). Then, a Partial Least Squares-Discriminant Analysis (PLS-DA) model was built to predict the asbestos presence in unknown samples (Bonifazi et al., 2019b). To this aim, the dataset was splitted into two parts using the Kennard-Stone (K-S) algorithm, keeping the replicates together: 70% of the spectra (i.e., 70% of the samples) was used in calibration, while the remaining part (30%) was used as the validation set. To assess the performance, the right number of Latent Variables (LVs) and generalizability of a predictive model, Venetian blinds (VBs) was adopted as cross-validation

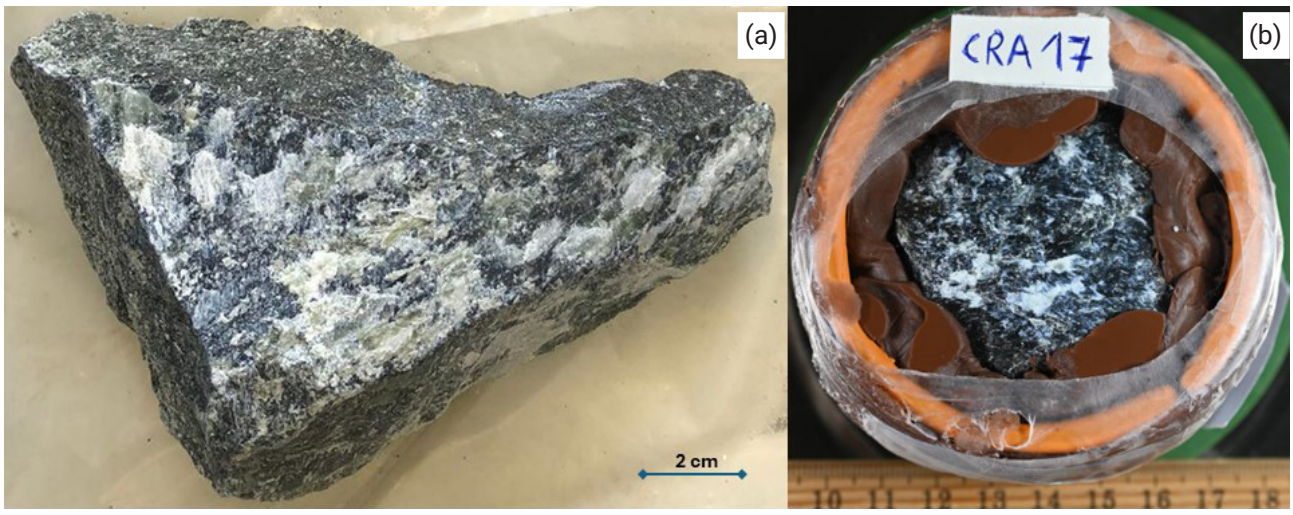

FIGURE 1: Sample named CRA_17 acquired on field (a) and in laboratory (b).

algorithm across different subsets of data. The goal of cross-validation is to ensure that the model will perform well on unseen data, rather than just on the data it was trained on.

The classifier performance was evaluated using the parameters calculated from the confusion matrix, that compare the True Positives (TP), the False Positives (FP), the True Negatives (TN) and the False Negatives (FN) results. The resulting parameters are:

- Precision = $TP/(TP+FP)$
- Sensitivity = $TP/(TP+FN)$
- Specificity = $TN/(TN+FP)$
- Accuracy = $(TP+TN)/(TP+FP+TN+FN)$

3. RESULTS AND DISCUSSION

3.1 Conventional techniques

3.1.1 Stereomicroscopy

As expected, the rock fragments present colors ranging from light up to dark green and they often show translucency and present strongly altered surfaces, partially covered by white aggregates, and isolated translucent fragments (Figure 2a). The latter frequently show straight edges and shapes, that are different from those typically exhibited by chrysotile bundles (Figure 2b).

Also focusing on the aggregates, translucent elongated minerals are noticed, embedded in a white matrix, the latter composed by fine granules that resemble talc (Figure 2c). In most cases these fibers are poorly resolvable and difficult to classify. However, they frequently show morphological characteristics like the isolated fragments. Also, Man-Made Vitreous (MMV) fibers are frequently found, especially in samples collected at the excavation face, where fiberglass bars were used to reinforce it. MMV fibers are easily distinguishable, because the diameters vary from 30 to 50 µm and the shapes are quite always regulars (Figure 2d).

At high magnifications (around 100X), few Asbestiform Fibers (AFs) can be found, which are clearly referrable to chrysotile (Figure 3). The number of AFs per each sample is reported in Table 2. The values range from 0 to 25 (CRA_17) with an average equal to 3 fibers per sample. They are present in 16 of 22 samples, in most cases within the whitish aggregates. As expected, no asbestiform fibers have been found in the uncontaminated internal storage.

3.1.2 Analysis of the fine fraction

Results concerning only the external storage are here presented. Chrysotile fibers and bundles have been found in the composed sample. A SEM image and the EDS spectrum of a typical one are reported in Figure 4. In the same figure, granular fragments are notable, which show the same elemental composition as chrysotile. These fragments belong to not-fibrous serpentines (e.g., lizardite, antigorite) and have been frequently found in the samples (Figure 5). Since the latter show often strongly elongated shapes, to conduct an accurate morphological analysis is crucial to obtain precise and reliable results. It seems, however, that using SEM-EDS alone to classify chrysotile and other serpentines can cause misclassification errors, when the particle dimensions fall below approximatively 0.2 µm, as regards thickness, and 10 µm for the lengths (see the small, elongated particles in Figures 4 and 5). Indeed, the

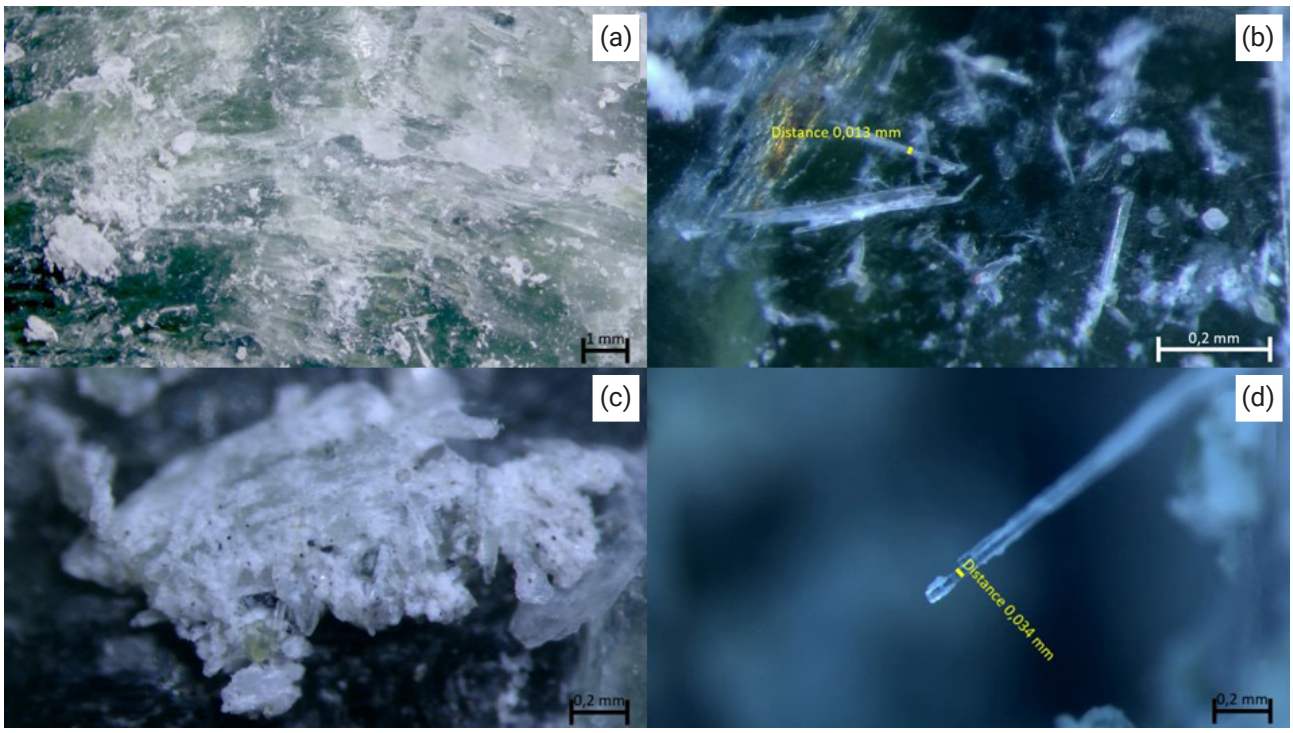

FIGURE 2: Typical surface exhibited by a serpentinite at 7.8X (a); elongated (b) and aggregated (c) mineral particles, and Man-Made Vitreous Fiber at 50X (d).

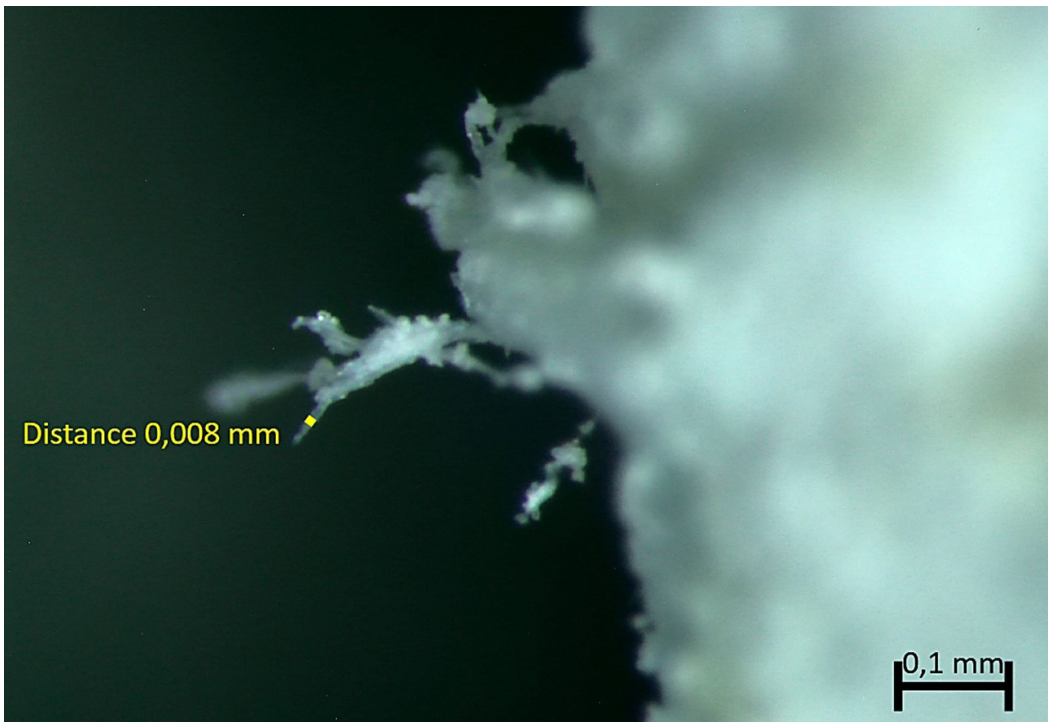

FIGURE 3: Chrysotile fibers covered by white fine granules at 100X.

TABLE 2: Number of asbestiform fibers for each sample.

Sample ID	Sampling area	Chrysotile fibers (N)
CRA01	External deposit	1
CRA02	External deposit	2
CRA03	External deposit	0
CRA04	External deposit	4
CRA05	External deposit	2
CRA06	External deposit	5
CRA07	External deposit	1
CRA08	External deposit	N.A.
CRA09	External deposit	1
CRA10	External deposit	0
CRA11	External deposit	2
CRA12	External deposit	0
CRA13	External deposit	0
CRA14	External deposit	1
CRA15	Quarry front	1
CRA16	Quarry front	0
CRA17	Quarry front	25
CRA18	Quarry front	4
CRA19	Quarry front	4
CRA20	Quarry front	4
CRA21	Internal deposit with asbestos	3
CRA22	Internal deposit without asbestos	0
CRA23	Internal deposit with asbestos	6
CRA24	Quarry front	N.A.

state-of-art analytical technique is the Transmission Electron Microscopy (TEM), but it is even more time-consuming and complex than SEM. The reported results are consistent with the scientific and normative literature (Malinconico et al., 2022; Militello et al., 2019).

3.2 Reflectance spectroscopy analysis

3.2.1 Pre-processing

The average spectra of the samples acquired on-site are shown in Figure 6. The same figure also shows the spectra averaged by the presence/absence of AFs, as resulting from stereomicroscopy analysis. Figure 7, instead, shows the pre-processed spectra of the two classes (“Presence of AFs” and “Absence of AFs”).

3.2.2 Principal Component Analysis

The scores plot of the PCA model conducted with two principal components is showed in Figure 8. The model captured the 89% of the total variance. The uncontaminated samples are grouped mainly in the first quadrant (i.e., negative PC1 and positive PC2 spaces), due to reflectance variations within the 1400-1420 nm and 2345-2365 nm ranges (see the loadings plot in Figure 9). Such spectral ranges include both: i) weak absorption features related to the common peaks of silicates and ii) one strong absorption caused by carbonates near 2350 nm (Clark et al., 1990). As expected, the scores of the contaminated samples are more spread and difficult to interpret. In this case, some samples are well separated from the uncontaminated ones by the strong absorptions that almost all silicates exhibit within the 1380-1400 nm range and around 1900 nm (Clark et al., 1990). The influence of mineral-specific

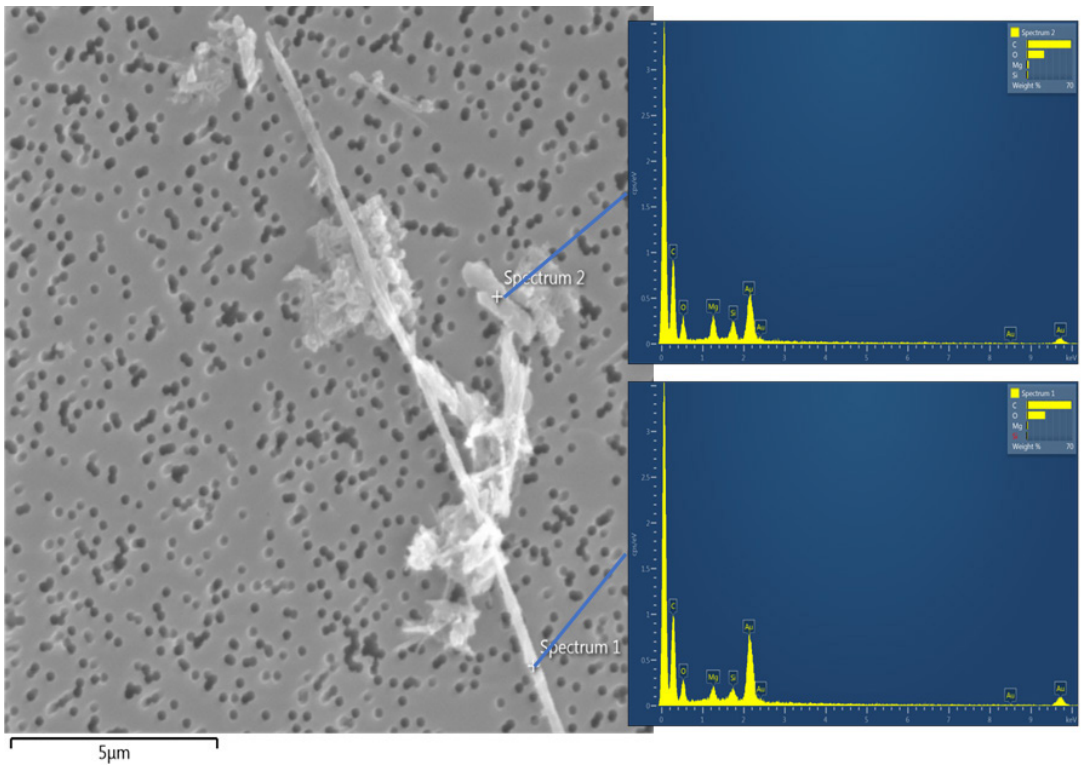

FIGURE 4: SEM image and EDS spectra of a chrysotile fiber (1) and not-fibrous serpentine fragments (2). The carbon signal comes from the underlying adhesive tab.

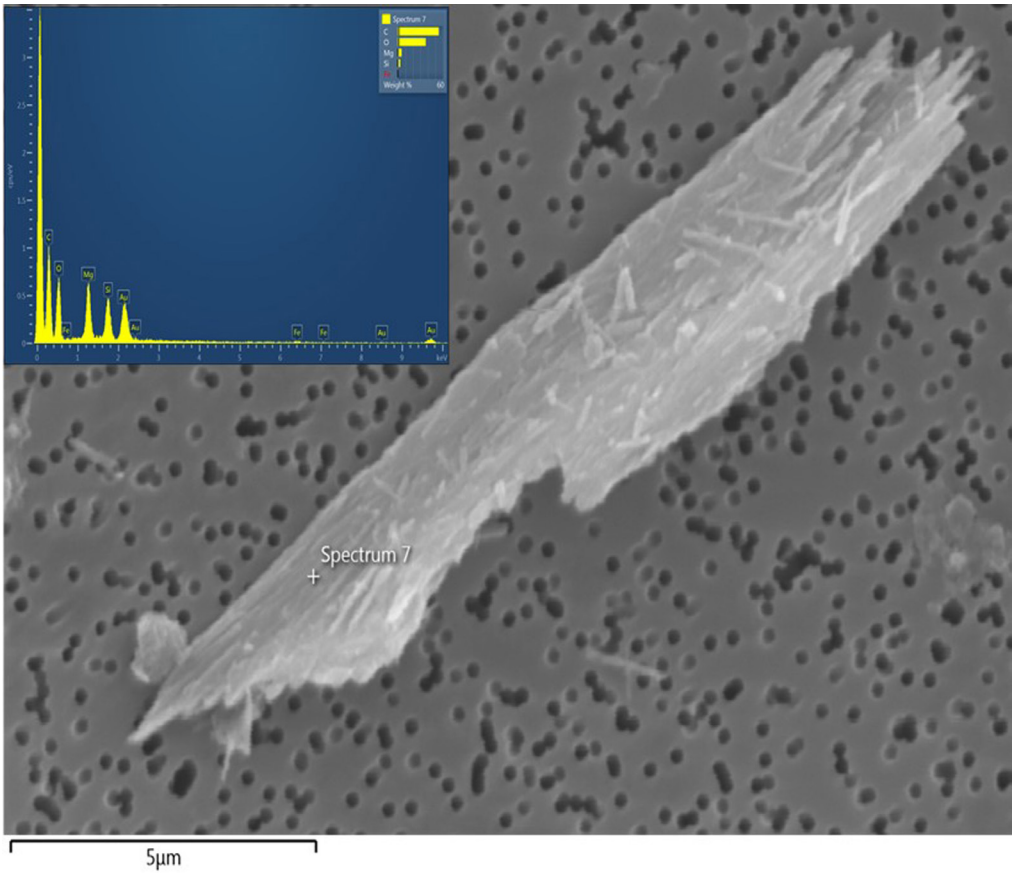

FIGURE 5: SEM image and EDS spectrum of a not-fibrous serpentine fragment and several unclassified small particles. The carbon signal comes from the underlying adhesive tab.

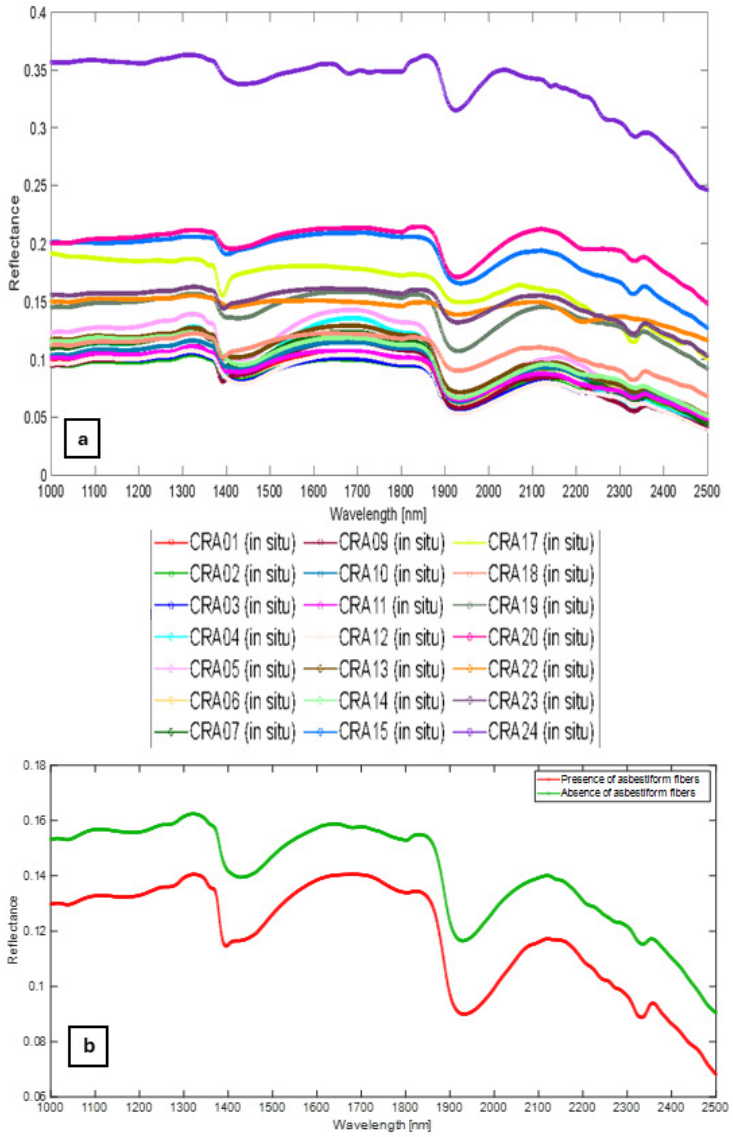

FIGURE 6: Reflectance spectra (1000-2500nm) of the samples acquired in situ averaged for: a) identification of the samples, b) presence/absence of AFs detected with stereomicroscopy.

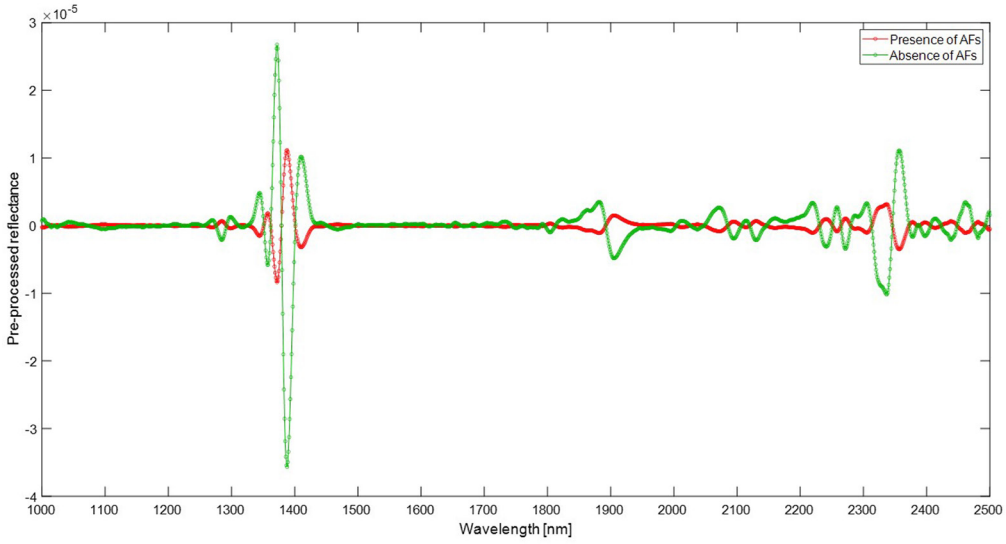

FIGURE 7: Pre-processed spectra averaged by presence/absence of AFs.

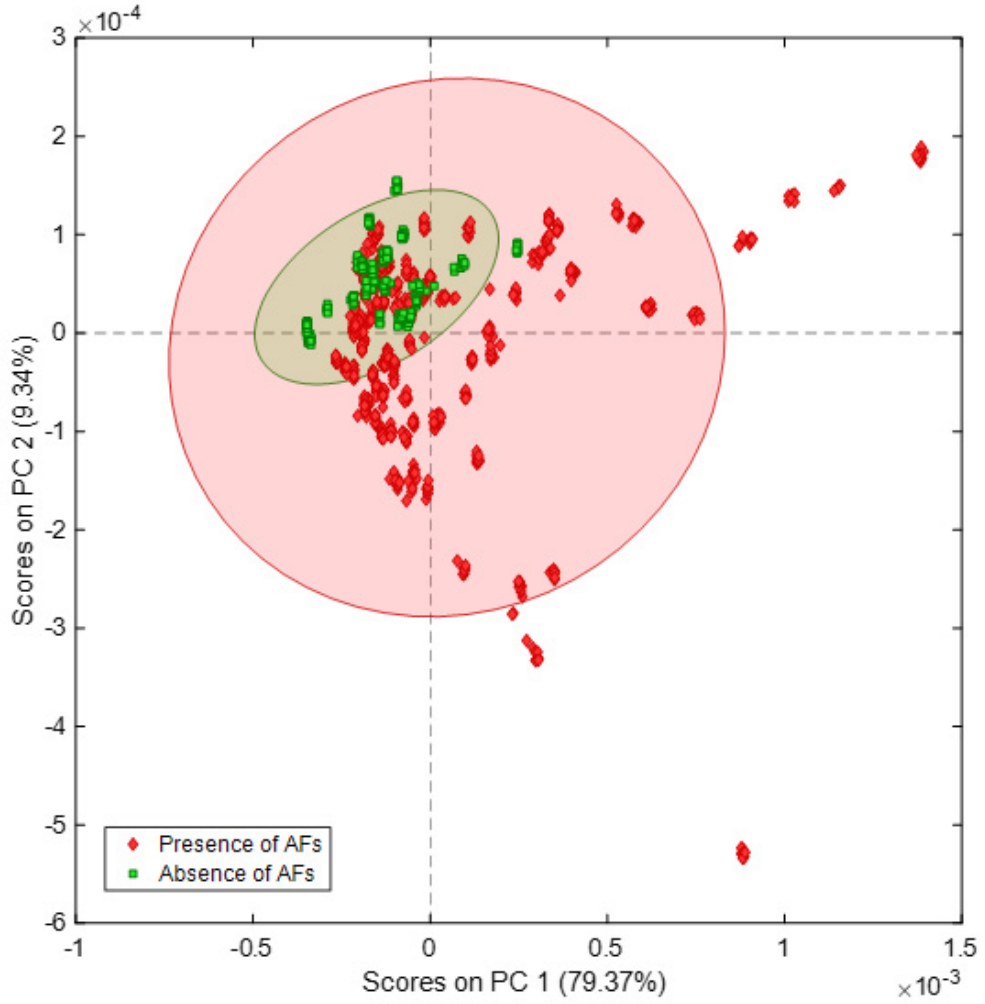

FIGURE 8: PCA Scores plot for spectra acquired on-site and grouped by presence/absence of AFs.

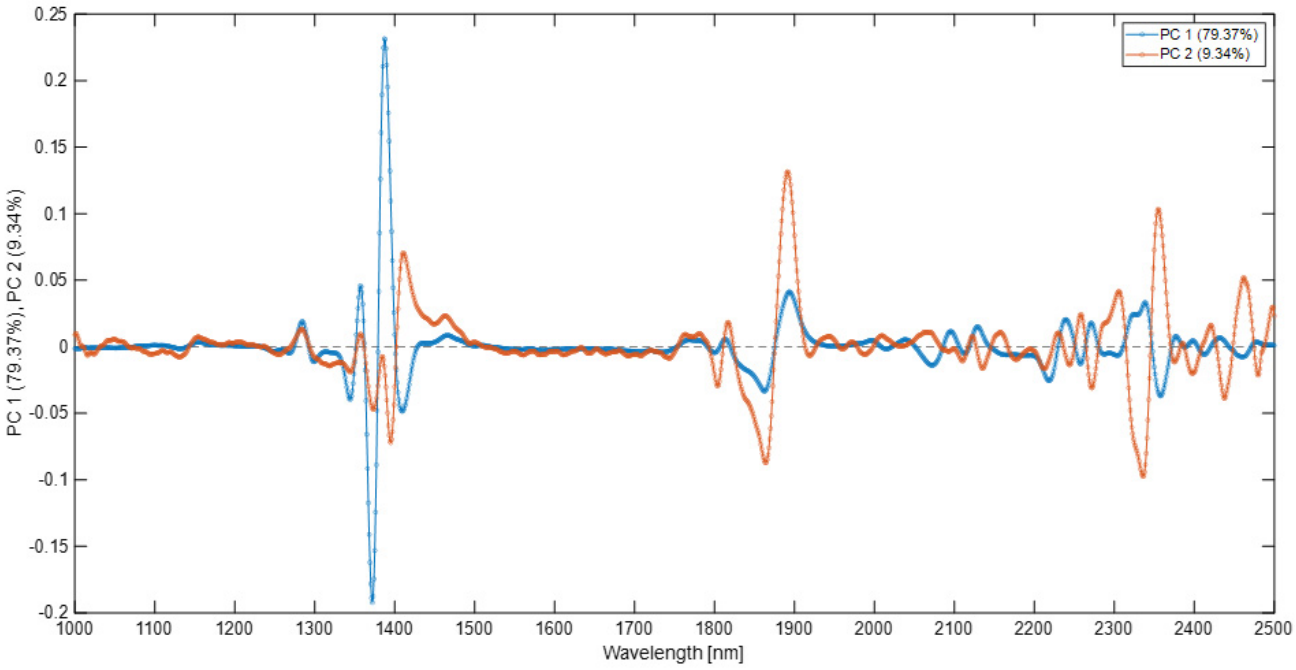

FIGURE 9: Loadings plot of the first two principal components of the on-site dataset.

TABLE 3: Confusion matrix of the PLS-DA model applied to the spectral dataset acquired on-site.

Model phase	Class	Sensitivity	Specificity	Precision	Accuracy	Error	N. of spectra
Calibration	Presence of asbestiform fibers	0.948	0.970	0.995	0.951	0.049	650
	Absence of asbestiform fibers	0.970	0.948	0.740	0.951	0.049	100
Cross-validation	Presence of asbestiform fibers	0.946	0.960	0.994	0.948	0.052	650
	Absence of asbestiform fibers	0.960	0.946	0.733	0.948	0.052	100
Validation	Presence of asbestiform fibers	0.633	0.173	0.434	0.403	0.597	150
	Absence of asbestiform fibers	0.173	0.633	0.321	0.403	0.597	150

absorptions in the variance should be better assessed in future studies.

3.2.3 PLS-DA model

It can be seen in Table 3 (confusion matrix) that the two-class model works very well in both calibration and cross-validation. Instead, the asbestos-free samples CRA10, CRA13 and CRA03, and the sample CRA14 (only one AF found) are not correctly classified in the prediction phase.

Finally, the Variable Important in Prediction (VIP) scores plot are reported in Figure 10. Also in the classification model, the most important wavelengths are related to absorptions that are typically showed by silicates (near 1380 nm, 1880 nm and 2330 nm) and carbonates (2350 nm) (Clark et al., 1990).

4. CONCLUSIONS

This document reports the preliminary results of a study conducted to automatically classify the asbestos-contaminated tunnel spoils produced during the excavation of a new high-speed and great capacity railway from Genoa to Milan.

Twenty-four samples were collected and analyzed with an innovative approach that exploits on-site spectroscopy coupled with chemometrics and calibrated through microscopy techniques. In more detail, the classification model was trained with qualitative data obtained by means of stereomicroscopy and partially supported by electron microscopy. At this phase of the project, the results are promising because both specificity and sensitivity values in the model cross-validation are around 95%. Hence, on-site reflectance spectroscopy coupled with chemometrics

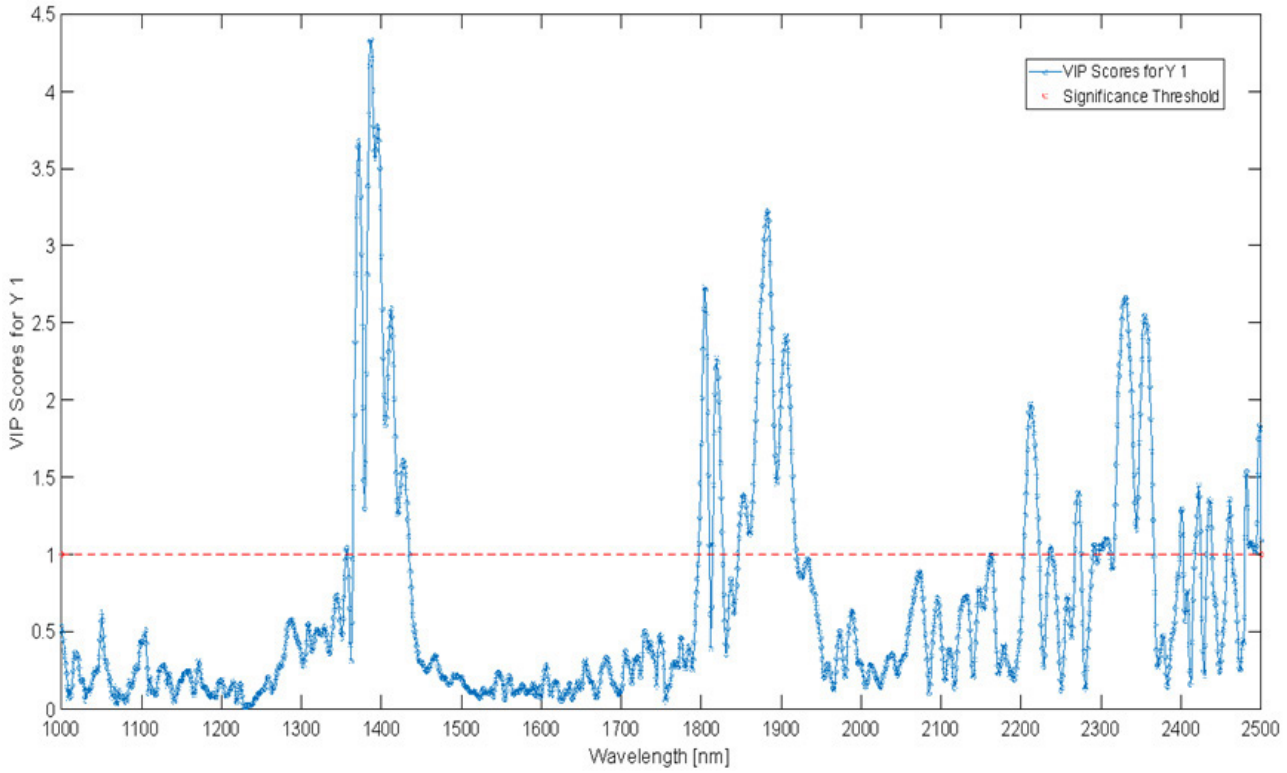

FIGURE 10: VIP scores of the PLS-DA model as a function of wavelengths.

show to us a good potential for real-time discrimination of asbestos presence in GS tunnel spoils. There is a need for in-depth research to demonstrate, on a more substantial analytical and statistical basis, the validity of this innovative sensor-based methodology and, specifically, to achieve an estimation of the asbestos concentration within the samples.

ACKNOWLEDGEMENTS

Thanks are due to the Pizzarotti-Collini consortium - Webuild of Cravasco railway tunnelling site (Genoa - Italy) in the persons of Stefano Fiori and Luca Fronza for their collaboration during the on-site survey and subsequent safety discussions.

REFERENCES

Bloise, A., Critelli, T., Catalano, M., Apollaro, C., Miriello, D., Croce, A.,... Belluso, E. (2014). Asbestos and other fibrous minerals contained in the serpentinites of the Gimigliano-Mount Reventino Unit (Calabria, S-Italy). Environmental Earth Sciences, 71(8). https://doi.org/10.1007/s12665-013-3035-2

Bonifazi, G., Capobianco, G., Palmieri, R., & Serranti, S. (2019a). Hyperspectral imaging applied to the waste recycling sector. Spectrosc. Eur, 31, 8-11. https://doi.org/https://doi.org/10.1255/sew.2019.a3

Bonifazi, G., Capobianco, G., & Serranti, S. (2019b). Hyperspectral imaging and hierarchical PLS-DA applied to asbestos recognition in construction and demolition waste. Applied Sciences (Switzerland), 9(21). https://doi.org/10.3390/app9214587

Carmignano, O., Vieira, S., Brandao, P., Bertoli, A., & M. Lago, R. (2019). Serpentinites: Mineral Structure, Properties and Technological Applications. Journal of the Brazilian Chemical Society, 31. https://doi.org/10.21577/0103-5053.20190215

Clark, R. N., King, T. V. V., Klejwa, M., Swayze, G. A., & Vergo, N. (1990). High spectral resolution reflectance spectroscopy of minerals. Journal of Geophysical Research: Solid Earth, 95(B8), 12653-12680. https://doi.org/https://doi.org/10.1029/JB095iB08p12653

IMH - Italian Ministry of Health (1994). Decree 06 September 1994 Technical rules and methodologies for application of Art. 6 Part 3 and Art. 12 Part 2 of Law no. 257 of 27 March 1992, relative to asbestos ban.

Lee, R. J., Strohmeier, B. R., Bunker, K. L., & Van Orden, D. R. (2008). Naturally occurring asbestos-A recurring public policy challenge. In Journal of Hazardous Materials (Vol. 153).

Malinconico, S., Paglietti, F., Serranti, S., Bonifazi, G., & Lonigro, I. (2022). Asbestos in soil and water: A review of analytical techniques and methods. J Hazard Mater, 436, Article 129083. https://doi.org/https://doi.org/10.1016/j.jhazmat.2022.129083

Militello, G. M., Bloise, A., Gaggero, L., Lanzafame, G., & Punturo, R. (2019). Multi-analytical approach for asbestos minerals and their non-asbestiform analogues: Inferences from host rock textural constraints. Fibers, 7(5). https://doi.org/10.3390/fib7050042

IMT - Italian Ministry of Infrastructure and Transports (2024). Commissario Terzo Valico, Nodo ferroviario di Genova e Campasso. Retrieved 21 February from https://terzovalico.mit.gov.it/

Neo, E. R. K., Yeo, Z., Low, J. S. C., Goodship, V., & Debattista, K. (2022). A review on chemometric techniques with infrared, Raman and laser-induced breakdown spectroscopy for sorting plastic waste in the recycling industry. Resources, Conservation and Recycling, 180, 106217. https://doi.org/https://doi.org/10.1016/j.resconrec.2022.106217

Olori, A., Di Pietro, P., & Campopiano, A. (2017). Main interfering in spectroscopic analysis for the determination of asbestos containing materials (ACM). Italian Journal of Occupational and Environmental Hygiene, 8(3), 71-119. https://doi.org/10.36125/ijoehy.v8i3.251

Paglietti, F., Malinconico, S., della Staffa, B. C., Bellagamba, S., & De Simone, P. (2016). Classification and management of asbestos-containing waste: European legislation and the Italian experience. Waste Management, 50. https://doi.org/10.1016/j.wasman.2016.02.014

Voit, K., Murr, R., Cordes, T., Zeman, O., & Bergmeister, K. (2020). Tunnel spoil recycling for concrete production at the Brenner Base tunnel in Austria. Structural Concrete, 21(6), 2795-2809. https://doi.org/https://doi.org/10.1002/suco.202000434

Webuild-RFI. (2021). Genoa-Milan: the high-speed train route running below the mountains. Retrieved 02 May 2024 from https://www.webuildvalue.com/en/stories-behind-projects/the-terzo-valico-amid-the-mountains.html

Wold, S., Esbensen, K., & Geladi, P. (1987). Principal component analysis. Chemometrics and intelligent laboratory systems, 2(1-3), 37-52. https://doi.org/https://doi.org/10.1016/0169-7439%2887%2980084-9